XLIII CILAMCE
21–25, November, 2022
FOZ DO IGUAÇU – PR – BRAZIL

A thermo-mechanical DEM framework for the simulation of selective laser sintering

Osvaldo D. Quintana-Ruiz[1], Eduardo M.B. Campello[1]

[1]*Dept. Structural and Geotechnical Engineering, Polytechnic School, University of São Paulo*
P.O. Box 61548, 05424-970, São Paulo, SP, Brazil
quintana.ruiz@usp.br, campello@usp.br

Abstract. This work presents a simple thermo-mechanical model based on the Discrete Element Method (DEM) for the rapid simulation of SLS processes. Our approach combines the DEM with lumped heat transfer equations to describe the various thermal phenomena that may take place when the particles are excited by external heat sources such as laser beams. We consider the essential ingredients that are relevant to the problem, such as inter-particle contact and bonding, heat transfer (through conduction, convection and radiation) as well as phase transformation due to high temperature changes (which may be critical in certain applications). The model is relatively simple and straightforward to be implemented by engineers and analysts interested in the field, and may be a useful tool for practical, rapid process simulation, design, and analysis. Numerical examples are provided to illustrate the practical use of the proposed framework for the simulation of SLS advanced manufacturing processes.

Keywords: particles, thermo-mechanical effects, 3D printing, discrete element method

1 Introduction

In the last years, modern industry (such as in aerospace, automotive and biomedical fields, to cite just a few) has incorporated Additive Manufacturing (AM) techniques as a fast and efficient alternative for the manufacture of industrial parts. These processes allow the production of 3D large-scale complex structures offering the chance of the production of customized parts, sometimes with individualized properties, and with a remarkable reduction of material usage. This technology came about as a result of developments in a diversity of different technology sectors, for example: computing power, control, and the improvement on the design of many kinds of subdevices used in AM processes. Also, the advances in the structural design, like topology optimization, constitutes a key point that enables to a better use and take advantage of all the capabilities of this technology. Many of the earliest AM systems were based on laser technology and until now, continue as an ideal candidate as long as this technology requires material in each layer to be solidified or joined in a selective manner.

Selective Laser Sintering (SLS) is an AM technique whereby powder particles are sintered (or partially fused) through an external heat source (typically, a laser beam). According to Milewski [1], in SLS process, a heat source is used to break up surface oxides to bring atoms and molecules close enough to allow diffusion and grain growth to form metallic bonds between the particles. The final microstructure is created under a controlled porosity, and the void volume or un-sintered spaces will depend upon the material, temperature, pressure, and time. This technology was the first commercialized Powder Bed Fusion (PBF) technique and originally was developed to produce plastic prototypes using a point-wise laser. According to Gibson et al. [2], this approach was subsequently extended to metal and ceramics powder and is very popular nowadays in the industry – reason why it is one that we opt to focus here. With this technique, becomes easier to print alloys containing materials with different melting points, or even combine two different materials, like metal and plastic materials (e.g., alumide, which is a mixture of nylon powder and aluminum powder) and since the SLS technique does not fully melt the metal, less energy is required in the process. Another common technique in AM is the Selective Laser Melting (SLM), where the metal powder particles fully melt and fuse to each other to create a solid part. However, unpredictable properties of the final manufactured product remain as one of the main barriers to adoption of AM (including SLS).

2 Simulation of a metal manufactured prototype ring using SLS process

In the following example, we use a DEM formulation by the authors (see [3] [4] [5]) simulate a sintering-based AM process to build a ring-like part of mean diameter $d = 1.0\,\text{mm}$ (see Figure 1a). A sample of metallic powder is randomly generated with particle sizes following a Gaussian distribution with a mean diameter of $\bar{d} = 27\ \mu\text{m}$ and std. dev. of $3.5\ \mu\text{m}$ (the distribution is truncated at three std. dev. from the mean such that all diameters lie in the interval $[16.5\,\mu\text{m},\ 37.5\,\mu\text{m}]$) resulting in $NP = 12000$ particles. The particles were deposited by gravity onto a rigid surface and allowed to settle, as to form a 2 mm × 2 mm square bed domain. The chosen material for the metallic powder particles is the 316L stainless steel (316L SS), which is usually adopted by manufacturers in SLS processes. The material properties (mechanical and thermal) for 316L SS as a function of temperature and phase are depicted in Table 1 (values in between the specified ranges are obtained through Lagrangian interpolation). To consider the phase transformation, we follow the same model of Ganeriwala and Zohdi [6] [7]. Other parameters used in the simulation are given in Table 2. The type of laser used was the Gaussian laser beam with a cross-sectional diameter of $d = 0.24$ mm scanning over the particle bed with a constant velocity of 4000 rad/s and following a circular pattern motion (see, Figure 1b). The time-step size adopted, considering that the particles are very stiff, was of $\Delta t = 2\times10^{-8}$ s for the initial deposition stage and $\Delta t = 5\times10^{-9}$ for the laser sintering stage, taking into account that we are considering phase transformation of the material. The beam is allowed to scan for four laps, and the total simulation time was of $t_F = 6.28\times10^{-3}$ s. An inert gas is considered as the surrounding atmosphere of the simulation. This is a typical practice in SLS processes to avoid oxidation that would affect the melting and consolidation of the metal particles. The computation time required for the simulation is about 0.085 hours per each 6.28×10^{-5} s of the problem´s duration in a standard, single processor laptop computer (at 2.30 GHz) with no parallelization nor usage of the graphics processing unit.

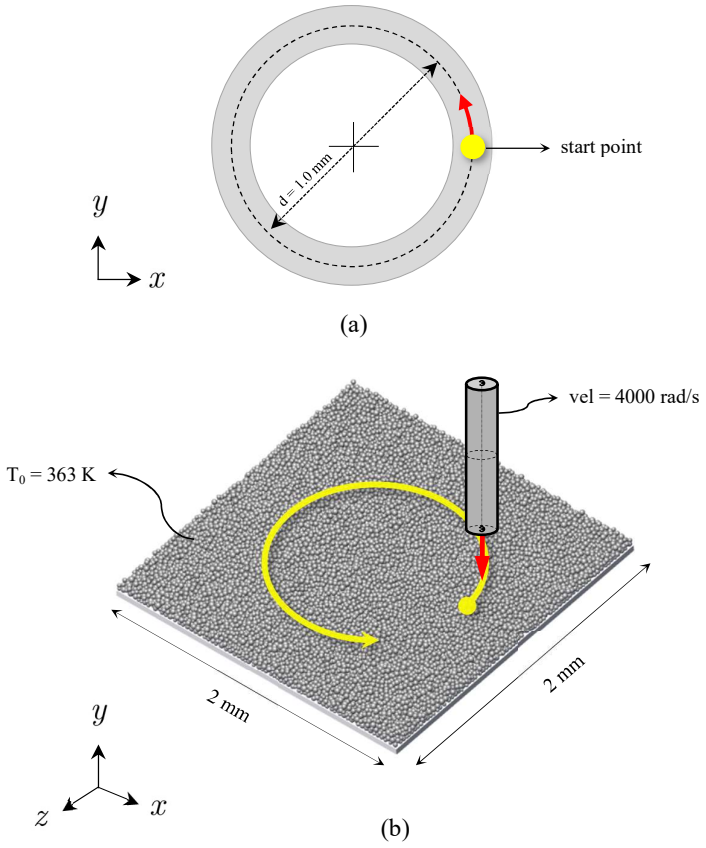

Figure 1. Laser-sintering of a prototype metal ring. Problem definition.
a) Top view b) Isometric view

Table 1. Material properties for 316L SS as a function of temperature.
Source: AK Steel [8]

Temperature (K)	Specific heat (J/kg K)	Thermal conductivity (W/m K)	Density (kg/m^3)	Elasticity modulus (GPa)
293	452	13.3	7952	198
366	485	14.3	7919	194
478	527	15.9	7877	185
589	548	17.5	7831	177
700	565	19.0	7786	167
811	573	19.8	7739	157
922	586	21.9	7692	148
1033	615	23.2	7640	137
1144	649	24.6	7587	129
1255	690	26.2	7537	120
1700 (liquid)	815	32.4	7300	1.70×10^{-6}

Table 2. Parameters used in the simulation

Nº	Parameter	Values
1	Particles´ elastic modulus (room temperature) and Poisson's ratio	198 GPa and 0.26
2	Particles´ friction and rolling resistance coeffs.	0.5
3	Particles´ contact and friction damping rates	0.9
4	Adhesion parameters (see [4]) ξ^{bond}, α^{adh} and $\varepsilon_{ij,\mathrm{eq}}$	1.0, 1.0 and 0.01
5	Sintering, melting and boiling temperature	1200K, 1700 K and 3130 K
6	Latent heat of melting	2.99×10^5 J/kg
7	Latent heat of vaporization	6.09×10^6 J/kg
8	Material emissivity and absorptivity	0.33
9	Laser scan speed	4000 rad/s
10	Laser spot size	120 μm
11	Powder bed porosity	0.55
12	Preheat particles´ temperature	363 K
13	Environment temperature	363 K
14	Temperature amplitude for phase transformation	170 K (10% of melting temperature)

To track the motion of the particles and their thermal states over time under the influence of body (e.g. gravitational) forces, contact and friction forces (and the related moments w.r.t the particles´ centers), rolling resistance effects, heat transfer through conduction (at the particles´ interfaces upon contact with other particles), convective cooling and radiative effects, we follow the thermo-mechanical formulation of previous works of the authors, Quintana-Ruiz and Campello [3] [9]. To consider the thermal energy that hits a particle from the laser beam we compute an intensity function depending on the particle's position w.r.t. the device´s (or beam´s) center. This function is as follows

$$I_i^{dev}(\lambda_i, z_i) = I_0 A_i e^{-\mu z_i} e^{(-2\lambda_i^2/w^2)}, \tag{1}$$

where I_0 is the peak intensity, $A_i = \pi r_i^2$ is the particle´s frontal area, λ_i is the radial distance between the center of the beam and particle i, μ is the attenuation coefficient, which gives a measure of how quickly an electromagnetic wave attenuates in the material, and w is the beam spot size (the radius of the beam itself). For the peak intensity, we write eq. (2), where P_0 is the nominal power of the laser in (W) and f is the distribution factor (i.e., a factor such that the energy becomes more focused with a higher value of f, see DebRoy [10]):

$$I_0 = \frac{fP_0}{\pi w^2}, \tag{2}$$

For powders and granular materials, the attenuation coefficient may be computed according to the theory of Gusarov et al. [11] [12]. It can be found in the literature by the name of optical extinction coefficient β . For spherical powder particles this value can be approximated as

$$\beta = \frac{3}{2}\frac{1-\phi}{\phi}\frac{1}{D}. \tag{3}$$

where ϕ is the porosity of the powder bed, and $D = 2r_i$ is the dimension of a typical particle. Other expressions for the device´s input power may be adopted, according to the problem at hand. For the adhesion force between particles, we compute the bonding in the normal direction according to the formulation proposed by the Campello and Quintana-Ruiz [4] and besides that, we include a tangential adhesion force and a rotational adhesion moment, such that

$$\boldsymbol{f}_{ij}^{bond,\tan} = k_{bond,\tan}\Delta\boldsymbol{x}_{ij}^{\text{trial}} - d^{bond,\tan}\boldsymbol{v}_{ij,t}\,, \tag{4}$$

where $\boldsymbol{f}_{ij}^{bond,\tan}$ is the adhesion force in the tangential direction and, $k_{bond,\tan}$ is the adhesion stiffness in the tangential direction, $\Delta\boldsymbol{x}_{ij}^{trial}$ is the pair´s trial adhesion deformation in the tangential direction and $d^{bond,\tan}$ is a friction tangential damping constant

$$d^{bond,\tan} = 2\xi^{bond}\sqrt{m^* k_{bond,\tan}}. \tag{5}$$

where ξ^{bond} is the damping rate of the oscillation and m^* is the effective mass of the pair $i-j$. For the rotational adhesion moment, we have

$$\boldsymbol{m}_{ij}^{bond,rol,\tan} = -k^{bond,rol,\tan}\Delta\boldsymbol{\theta}_{ij}^{\text{trial}} - d^{bond,rol,\tan}\boldsymbol{\omega}_{ij}, \tag{6}$$

where $\boldsymbol{m}_{ij}^{bond,rol,\tan}$ is the rotational adhesion moment, $\Delta\boldsymbol{\theta}_{ij}^{trial}$ is the pair´s trial adhesion rotation, $k^{bond,rol,\tan}$ is the stiffness of the rotational spring, and $d^{bond,rol,\tan}$ is a rolling damping constant, given by

$$k^{bond,rol,\tan} = k_{bond,\tan}(r^*)^2 \quad \text{and} \quad d^{bond,rol,\tan} = \xi^{bond}\sqrt{j^* k^{bond,rol,\tan}}, \tag{7}$$

where r^* is the effective radius and j^* is the rotational inertia of the pair $i-j$ w.r.t. its contact point. Moreover, we include a temperature criterion for bonding, whereby for a contacting pair $i-j$ the temperatures of both particle i and particle j must be higher than a specified critical temperature (which is the sintering temperature) for the bond to be activated between them[1]. According to Shi et al. [13], an appropriate scanning strategy contributes to reduce distortion, anisotropy and porosity on the final manufactured piece. Moreover, helps to define the proper hatch spacing (distance between laser passes), which is particularly important to avoid improper bonding between particles and undesired cooling and solidification. To assess some of these issues, we run a series of simulations varying the distribution factor f and the nominal power P_0 of the laser, while keeping the scanning speed fixed. Our interest is to find the ideal combination that will guarantee a proper bonding between particles, a coherent and uniform width of the ring, while ideally requiring less energy from the laser. The values of P_0 adopted in the simulation were: 100 W, 150 W, 200 W, with f varying from 1 up to 4 for each value of P_0 .

Figure 2 shows the final configurations for each case after four laps ($t_F = 6.28\times10^{-3}$ s). As expected, when the value of f increases the energy becomes more focused independently of the laser power. According to our model, the gas phase is reached when the temperature is higher than 3215 K. Figure 3 shows a side view of the bed at the end of the fourth lap for the cases where gas particles are observed. Figure 4 shows snapshots of the sintered piece as obtained with our simulations and Table 3 summarizes the average and maximum temperatures reached by the powder bed at the final lap. As we can see, the amount of particles with bonding directly depends on the power of the laser and the distribution factor. However, too high values may turn some particles into gas, and this could create an undesired entrapped porosity on the final manufactured piece.

[1] The same criterion is adopted by Xin et al. [15].

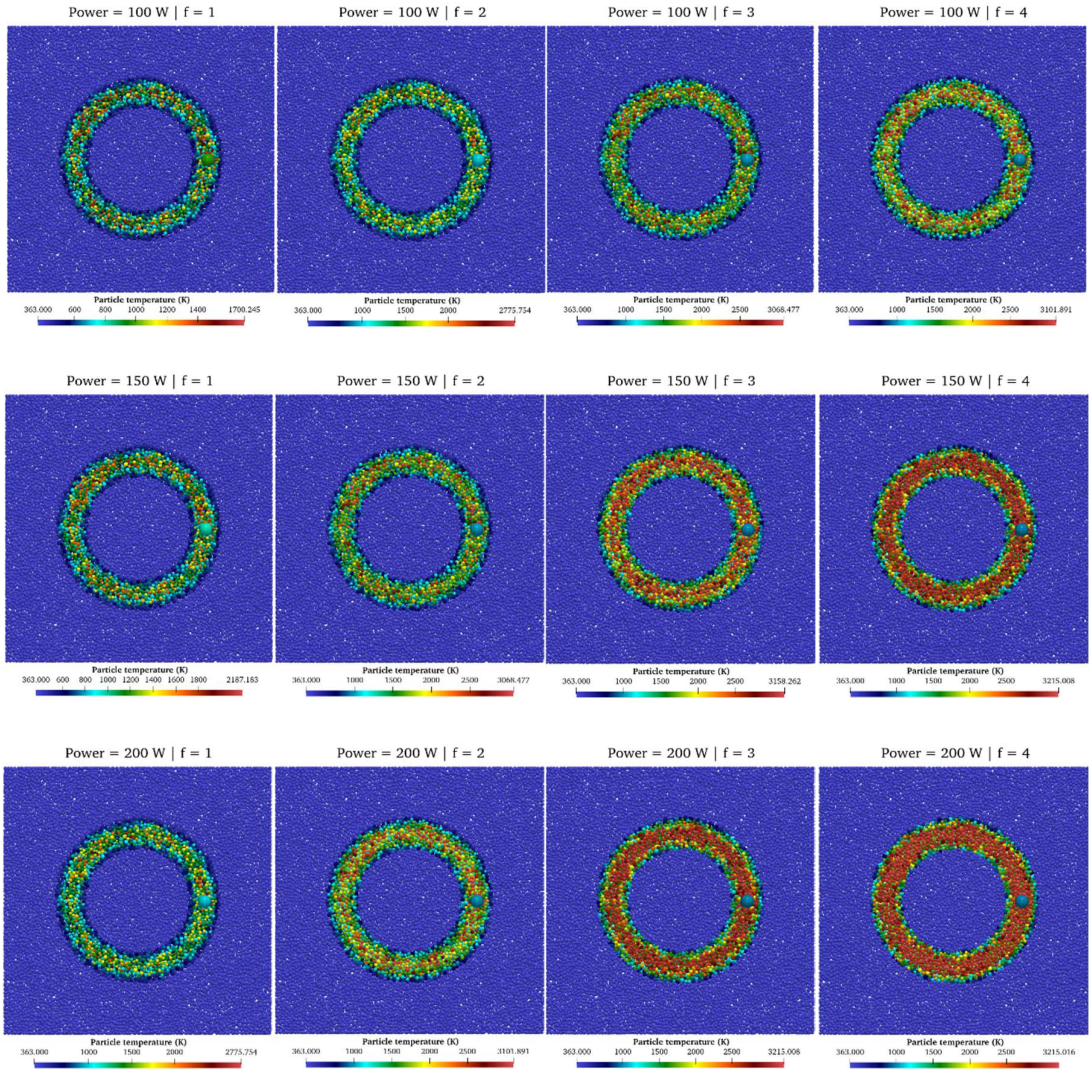

Figure 2. Temperature distribution of the powder bed as a function of laser nominal power and distribution factor at the end of the fourth lap ($t_F = 6.28 \times 10^{-3}$)

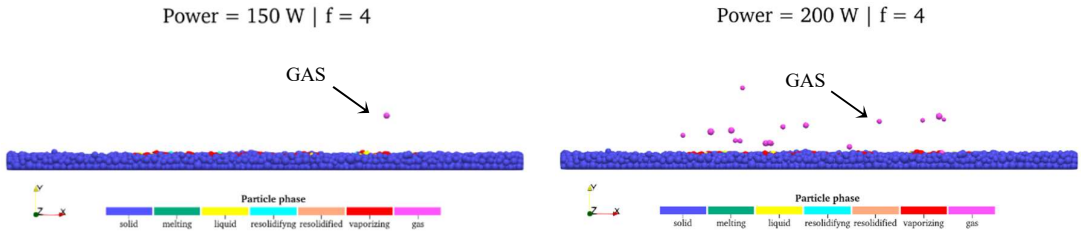

Figure 3. Side view of the powder bed for 2 cases showing particles with gas phase

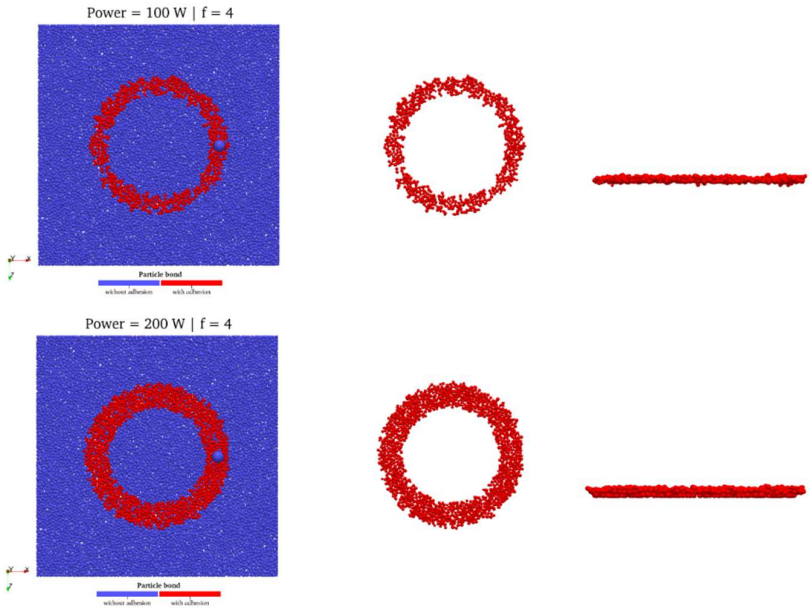

Figure 4. Final sintered piece after four laps for the cases with P_0 = 100 W and 200 W and f = 4. From left to right: top view of the particle bed, top view of the final piece (only bonded particles shown), side view of the final piece

Table 3. Summarized temperatures obtained in the simulation at the end of the fourth lap

Power (W)	Distribution factor (f)	Temperature (K)	
		Average	Maximum
100	1	421.861	1700.245
	2	469.193	2775.754
	3	510.517	3068.477
	4	544.580	3101.891
150	1	446.556	2187.183
	2	510.517	3068.477
	3	593.937	3158.262
	4	638.484	3215.008*
200	1	469.193	2775.754
	2	544.580	3101.891
	3	638.484	3215.008*
	4	676.584	3215.016*

* Gas phase

For the series of simulations presented in this example, we have varied the intensity and distribution factor of the laser and fixed the scanning velocity and the size of the particles, but our model has the flexibility to vary other parameters like the type of material, the scanning speed, and so on. The optimal set of parameters to be determined will depend on the material, geometry process parameters and purpose of the fabricated piece. The incorporation of genetic algorithms and machine learning as a tool for the optimization of AM processes are currently under development by the authors.

3 Conclusions

By the obtained results we found how the amount and distribution (w.r.t. the beam´s cross-section) of energy provided to the system influenced on the final number of particles with bonding and its effects on the quality of the final manufactured piece. This can be very helpful to identify the best set of parameters that will guarantee the

proper bonding between particles and the amount of energy that will be required. Moreover, this model allows us to study an optimal size distribution for the particles to ensure the maximum quantity of particles with adhesion without reaching an undesirable gas phase, which as we said before, will be increase the porosity. We believe that, with models of the type as proposed here, many AM industrial processes may be optimized, and experimental tests may be set up in a more oriented way.

Acknowledgements. First author acknowledges the postdoctoral funding from the Government of Paraguay through the National Scholarship Program for Postgraduate Studies Abroad Don Carlos Antonio López (BECAL), under the grant 72/2022. Second author acknowledges support by CNPq (Conselho Nacional de Desenvolvimento Científico e Tecnológico), Brazil, under the grant 313046/2021-2.

Authorship statement. The authors hereby confirm that they are the sole liable persons responsible for the authorship of this work, and that all material that has been herein included as part of the present paper is either the property (and authorship) of the authors, or has the permission of the owners to be included here.

4 References

[1] J. O. Milewski, Additive Manufacturing of Metals. From Fundamental Technology to Rocket Nozzles, Medical Implants, and Custom Jewelry, Springer, 2017.

[2] I. Gibson, D. Rosen and B. Stucker, Additive Manufacturing Technologies - 3D Printing, Rapid Prototyping , and Direct Digital Manufacturing, London: Springer, 2015.

[3] O. D. Quintana-Ruiz and E.M.B. Campello, "A coupled thermo-mechanical model for the simulation of discrete particle systems," *Journal of the Brazilian Society of Mechanical Sciences and Engineering,* vol. 42, no. 378, pp. 387(1-21), 2020.

[4] E.M.B. Campello and O.D. Quintana-Ruiz, "On a simple, stable and efficient bond model for inter-particle adhesion," *Computational Particle Mechanics,* Published online: 29 January 2021.

[5] E.M.B. Campello, "A computational model for the simulation of dry granular materials," *International Journal of Non-Linear Mechanics,* vol. 106, pp. 89-107, 2018.

[6] R. Ganeriwala and T. Zohdi, "Multiphysics modeling and simulation of selective laser sintering manufacturing processes," *Procedia CIRP 14. 6th CIRP International Conference on High Performance Cutting, HPC2014,* pp. 299-304, 2014.

[7] R. Ganeriwala and T. Zohdi, "A coupled discrete element-finite difference model of selective laser sintering," *Granular Matter,* vol. 21, pp. 18(1-15), 2016.

[8] AK Steel, "316/316L Stainless Steel Product Data Bulletin," [Online]. Available: https://www.aksteel.com/sites/default/files/2018-01/316316L201706_2.pdf. [Accessed April 2021].

[9] O. D. Quintana-Ruiz and E.M.B. Campello, "A thermo-mechanical formulation for the modeling of discrete particle systems," in *Ibero-Latin American Congress on Computational Methods in Engineering (XL CILAMCE)*, Natal, Brazil, 2019.

[10] T. DebRoy, H. L. Wei, J. S. Zuback, T. Mukherjee, J. W. Elmer, J. O. Milewski, A. M. Beese, A. Wilson-Heid, A. De and W. Zhang, "Additive manufacturing of metallic components – Process, structure and properties," *Progress in Materials Science,* vol. 92, pp. 112-224, 2018.

[11] A. V. Gusarov and J.-P. Kruth, "Modelling of radiation transfer in metallic powders at laser treatment," *International Journal of Heat and Mass Transfer,* vol. 48, no. 16, pp. 3423-3434, 2005.

[12] A. V. Gusarov, I. Yadroitsev, P. Bertrand and I. Smurov, "Model of Radiation and Heat Transfer in Laser-Powder Interaction Zone at Selective Laser Melting," *Journal of Heat Transfer,* vol. 131, no. 7, pp. 072101(1-10), 2009.

[13] Y. Shi, W. Zhang, Y. Cheng and S. Huang, "Compound scan mode developed from subarea and contour scan mode for selective laser sintering," *International Journal of Machine Tools and Manufacture,* vol. 47, no. 6, pp. 873-883, 2007.

[14] INCO databooks, "Reprinted from the publication "Mechanical and Physical Properties of the Austenitic Chromium-Nickel Stainless Steels at elevated temperatures," 1968. [Online]. Available: https://nickelinstitute.org/media/1637/austeniticchromium_nickelstainlesssteelsatelevatedtemperatures_mechanicalandphysicalproperties_2980_.pdf. [Accessed April 2021].

[15] H. Xin, W. Sun and J. Fish, "Discrete element simulations of powder-bed sintering-based additive manufacturing," *International Journal of Mechanical Sciences,* vol. 149, pp. 373-392, 2018.